Soft Matter

Accepted Manuscript

This is an *Accepted Manuscript*, which has been through the Royal Society of Chemistry peer review process and has been accepted for publication.

Accepted Manuscripts are published online shortly after acceptance, before technical editing, formatting and proof reading. Using this free service, authors can make their results available to the community, in citable form, before we publish the edited article. We will replace this *Accepted Manuscript* with the edited and formatted *Advance Article* as soon as it is available.

You can find more information about *Accepted Manuscripts* in the **Information for Authors**.

Please note that technical editing may introduce minor changes to the text and/or graphics, which may alter content. The journal's standard **Terms & Conditions** and the **Ethical guidelines** still apply. In no event shall the Royal Society of Chemistry be held responsible for any errors or omissions in this *Accepted Manuscript* or any consequences arising from the use of any information it contains.

Cyclic Behaviors of Amorphous Shape Memory Polymers

Kai Yu[1], Hao Li[1,2], Amber J.W. McClung[3], Gyaneshwar P. Tandon[4,5], Jeffery W Baur[5*],

H. Jerry Qi[1]*

[1]Woodruff School of Mechanical Engineering, Georgia Institute of Technology,

Atlanta, GA 30332, USA

[2]School of Civil Engineering, Hefei University of Technology, Hefei 230009, China

[3] Department of Mechanical Engineering, St. Mary's University, San Antonio, TX

78228, USA

[5]Materials and Manufacturing Directorate, Air Force Research Laboratory, WPAFB,

OH 45433, USA

[4]University of Dayton Research Institute, Dayton, OH, USA

*Author to whom correspondence should be addressed: jeffery.baur@us.af.mil;
qih@me.gatech.edu

Abstract: Cyclic loading condition is commonly encountered during the applications of shape memory polymers (SMPs), where the cyclic characteristics of the materials determine their performance during the service life, such as deformation resistance, shape recovery speed and shape recovery ratio, etc. Recent studies indicate that in addition to the physical damage or some other irreversible softening effects, the viscoelastic nature could also be another possible reason of the degraded cyclic behavior of SMPs. In this paper, we explore in detail the influence of the viscoelastic properties on the cyclic tension and shape memory (SM) behavior of an epoxy based amorphous thermosetting polymer. Cyclic experiments were conducted first, which show that although the epoxy material does not have any visible damage or irreversible softening effect during the deformation, it still exhibits obvious degradation in the cyclic tension and SM behaviors. A linear multi-branched model is utilized to assist in the prediction and understanding of the mechanical responses of amorphous SMPs. Parametric studies based on the applied model suggest that the shape memory performance can be improved by adjusting programming and recovery conditions, such as lowering the loading rate, raising the programming temperature, and reducing the holding time, etc.

Keywords: *Cyclic behavior; shape memory polymers; multi-branched model; viscoelasticity*

1. Introduction

Shape memory polymers (SMPs) are smart materials that have the ability to recover the permanent shape from one or sometimes multiple [1-3] predetermined temporary shapes after being exposed to an environmental stimulus, such as temperature [4, 5], magnetic field [6, 7], light [8, 9] and moisture [10] etc. This phenomenon is referred to as shape memory (SM) effect. In comparison with other SM materials like alloys and ceramics, SMPs exhibit unique properties, such as high programmable strain, light weight, low cost, etc., and hence gain extensive research interests in recent years for applications such as actuation components in microsystems, biomedical devices, aerospace deployable structures and morphing structures [11-13].

Whilst thermomechanical behaviors of SMPs were studied broadly in the past, their performance under cyclic loading conditions was relatively less explored. Theoretically speaking, for an intact polymer network, there should be no limit on the number of shape storage and recovery cycles the material can experience. However, some previous works have revealed degradation in both thermomechanical and SM behaviors of SMPs under cyclic working conditions, which are typically represented by a decreased shape recovery ratio or speed. One mechanism could be the damage in SMPs that resulted from fast loading, large deformation or low programming temperature [14-17]. For example, Gall et al [14] investigated the SM performance of an epoxy SMP by using micro-indentation. The results showed that indentation with high strain levels or at relatively low temperatures would increase the degree of

damage and consequently lead to incomplete recovery. The damage effect was also considered to be the main reason for degraded thermomechanical properties of SMP foams [18, 19]. In terms of polymer composites or structures, Ohki et al [15] studied the cyclic SM behavior of SMP composites filled with glass fibers, where the debonding failure between matrix resin and fibers would lead to unrecovered strain at the end of a SM cycle. Li et al. [20, 21] developed a new biomimetic self-healing system with cold-drawn SMP fibers providing driven force to close the wide-opened cracks in polymer matrix. There, the cyclic loss in the functionality of the SMPs fiber was interpreted as the damage process, and used to identify the state of the damage [22]. In the recent work by Shojaei et al.,[23] the damage mechanisms in SMPs were classified into mechanical damage [17, 19, 22, 24, 25] and functional damage [26-29]. The associated initiation and saturation of visco-plastic and damage was studied by using a consistent theoretical framework based on statistical mechanics.

In the aforementioned studies, damage introduced in SMPs or their composites leads to degradation in mechanical properties such as modulus, and consequently reduces the driving force for the shape recovery [30]. However, the question remains whether damage effect is responsible for all the observed deterioration of SM capability, or if other mechanisms also play a role. In the previous work by Tobushi et al [31, 32], a residual strain was observed after each loading or SM cycle. But this residual strain will gradually decrease during the subsequent stabilization step, which is more obvious under elevated temperatures. The change in unrecovered strain apparently will affect the measured shape recovery ratio in each SM cycle. Recently,

McClung et al. [33, 34] studied the thermomechanical and SM behaviors of a

Veriflex-E epoxy SMP, which exhibited viscous nature even at a temperature highly

above the transition temperature (T_g). The results showed that while the total shape

recovery ratio is gradually decreasing during the cyclic SM tests, the relative shape

recovery ratio, namely the amount of recovered strain in each shape memory cycle,

always approaches 100%. All these experimental investigations indicated that, in

addition to the damage effect, the viscoelastic properties of SMP could be another

possible reason for the performance decay in the cyclic behavior of SMPs.

In this study, we explore influence of viscoelastic properties on the cyclic

thermomechanical and SM behaviors of amorphous SMPs. A multi-branched model is

used to assist the discussions and help to explain the underlying mechanism. The

paper is arranged in the following order. Section 2 shows the experimental results of

the cyclic tension and SM tests on SMPs. Section 3 introduces the applied 1D

constitutive model. Section 4 presents comparisons and discussions between the

experimental results and the model predictions. The model is further utilized for

parametric studies, which reveal some strategies to improve the cyclic SM behavior

by properly selecting programming and recovery conditions of SMPs. The results for

these applications are also presented in Section 4.

2. Experimental Methods and Results

2.1 Materials

The SMP material used in this paper is a two-part Veriflex-E epoxy thermosetting

polymer, which was previously studied by McClung et al. [33, 34]. The resin was purchased from Cornerstone Research Group, Inc. (Dayton, Ohio, USA). During the synthesis, panels of neat resin were fabricated in sealed molds between two glass plates. The samples were cured in a convection oven following the manufacturer recommended cure cycle. The material was post-cured for 30 min at 150 °C before testing.

2.2. Dynamic mechanical analysis

Dynamic mechanical analysis (DMA) was performed by a DMA tester (Model Q800, TA Instruments, New Castle, DE, USA) to characterize the glass transition behavior of Veriflex-E epoxy SMP material. The rectangular sample (20mm×3.6mm×1mm) was first heated to 140 °C on the DMA machine and stabilized for 20min to reach thermal equilibrium, and then a preload of 1 KPa and an initial strain with a magnitude of 0.1 % was applied. During the experiment, the strain was oscillated at a frequency of 1 Hz with a peak-to-peak amplitude of 0.1 % while the temperature was decreased from 140 to 25 °C at a rate of 2 °C/min. The temperature in the chamber was held at 25 °C for 30 minutes and then increased to 140 °C again at the same rate. This procedure was repeated multiple times and the data from the last cooling step is reported in Fig. 1. The temperature corresponding to the peak of tan δ curve is shown to be 95.5 °C.
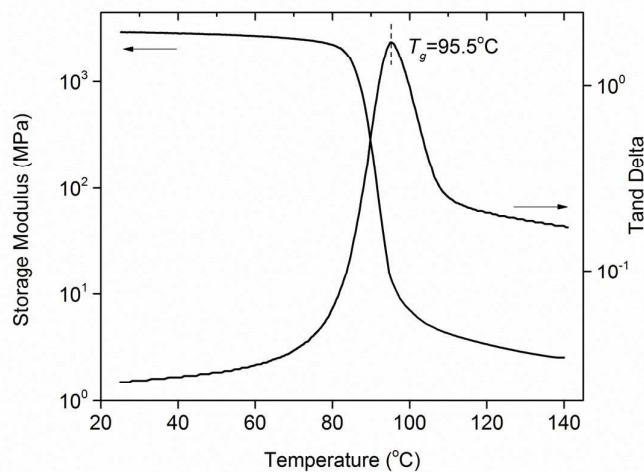
Figure. 1 Results of storage modulus and tanδ as functions of temperature from dynamic mechanical analysis test with heating rate being 2 $^{\circ}$C/min and frequency being 1HZ.

2.3 Cyclic tension tests

Cyclic tension tests were applied to examine the stress-strain behavior of the epoxy SMP. The tests were performed on the DMA machine with uniform sample dimension (15mm×3mm×1mm). Two groups of experiments were conducted. In the first group, the SMP sample was stretched by 60% (engineering strain) at 120 °C with a loading rate of 2%/s, and then followed by unloading at 2%/s until the stress reduced to zero. After each cycle, the SMP sample was stretched immediately without re-measuring the sample length. The target strain, loading and unloading rate were always identical in each loading cycle. Fig. 2a shows the stress-strain curves in the first ten loading cycles. It appears that the sample is softened after loading in view of the gradually reduced stress at the end of loading step. The residual strain is also seen to be increasing with the number of loading cycle, but it gradually saturates at about 15%.

In the second group of tests, another SMP sample was subject to cyclic tension

with the same target strain, testing temperature, loading and unloading rates. After each cycle, the sample was stabilized at 120 $^{\circ}$C for 20min, and its dimension was then re-measured dimension, which ensured that the loading stress-strain curve always starts from the origin in each cycle[35]. Fig. 2b shows the stress-strain curves in the first and tenth loading cycle. It can be seen that the stress-strain curves for these two cycles nearly coincide with each other, indicating no damage or irreversible softening effect within the polymer network. The results of these two sets of tests show that during the continuous loading test, the gradually decreased peak stress before unloading is due to the material viscoelasticity. The accumulated residual strain will lead to a gradually decreased real stretch in each loading cycle, and consequently a pseudo softening effect of the polymer network. If the residual stress could be removed (e.g. by long-time stabilization for recovery), the graph of each cycle will overlap closely, as shown in Fig. 2b.

(a)   (b)
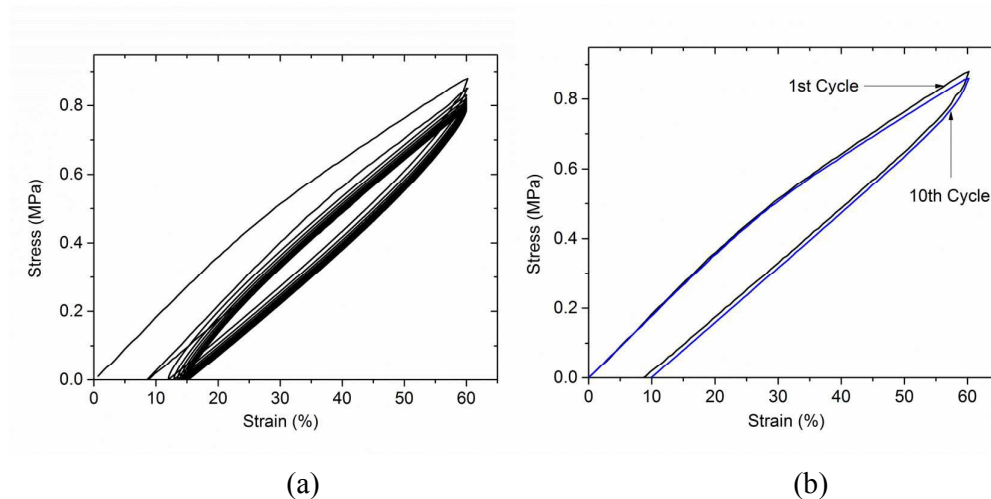
Figure 2. (a) The stress-strain curves in the first 10 loading cycles, without dimension measurement during the test. Temperature=120 °C, Loading rate=2%/s (b) The stress-strain curves in the 1st and 10th loading cycles. After each cycle, the material dimension is re-measured. Temperature=120 °C, Loading rate=2%/s.

2.4 Cyclic SM tests

Cyclic SM tests were conducted on an MTS machine (Model 312.21 with a 2.3-ton load frame) with a Thermotron temperature chamber (Model FR-3-CHM-LN2). Dumbbell shaped test specimens (total length = 115 mm, overall width = 19 mm, gage length = 25 mm, width of narrow section = 6 mm) were machined from the 3-mm thick panel according to ASTM-D 638(ASTM, American Society for Testing and Materials; Type IV). Strain control was accomplished by using an MTS laser extensometer with a 25.4-mm gage length of the retro-reflective tape applied to each sample.

The sample was first heated from 25°C to 130°C at a rate of 2.5°C/min, and then held for 60 min at 130°C. After that, the sample was strained to 60% (measured by the laser extensometer) with a loading rate of 50 mm/min by keeping the temperature at 130 °C. The sample was kept at the constant strain of 60% for 5 min. Next, the sample was cooled to 25°C at a rate of 2.5°C/min while the strain was kept at 60%, after which the sample was held (at 25°C and 60% strain) for 60 min to ensure thermal equilibrium in the sample. Subsequently, the mechanical load was removed from the sample at a rate of 50 mm/min. Once the force on the sample was released, the bottom grip was released from the sample, and free recovery was conducted on the sample while it was still mechanically held in the top grip to enable continuous strain measurements with the laser extensometer. The free recovery consisted of heating the sample (again at 2.5°C/min) to 130°C, keeping the temperature for 60 min, cooling the sample to 25°C (at 2.5°C/min), and finally holding the sample at 25°C for 60 min.

After each loading cycle, the SMP was subjected to the next SM cycle keeping the total programming strain as always 60%. The strain versus time during the recovery portion of the SM cycles 1, 2, 6 and 10 is plotted in Fig. 3. It also illustrates that the residual strain at the end of each cycle increases with the number of cycles, indicating a decay in the recovery of the SMP.
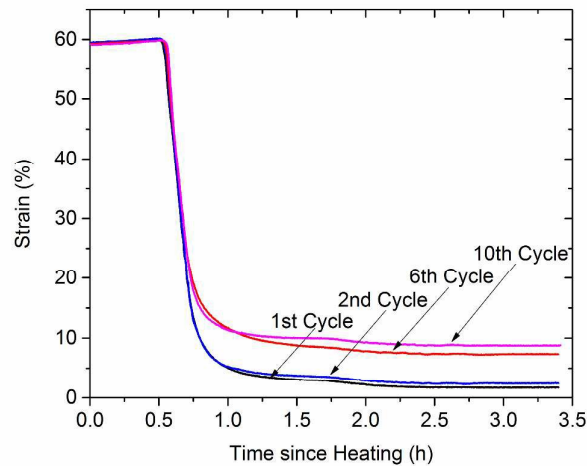
Figure 3. Variation of the strain during the cyclic SM test of 1, 2, 6, and 10 cycle. Programming temperature 130°C, loading rate 200%/min, holding time 5min, without length measurement after each SM cycle.

3. Constitutive Model

Here, a multi-branched constitutive model is used to assist the understanding of the mechanical responses of SMPs. We briefly present the constitutive model in this section. A detailed description can be found in Yu et al [30, 36-38], and the extended 3D constitutive relations can be found in Westbrook et al [39].

3.1 Overall Model Description

Fig. 4 shows the 1D rheological representation of the applied multi-branched model. The model consists of an equilibrium branch and several nonequilibrium

branches placed in parallel. The equilibrium branch is an elastic spring to represent

the equilibrium behavior of SMPs. Each nonequilibrium branch is a Maxwell element

with an elastic spring and a dashpot placed in series.
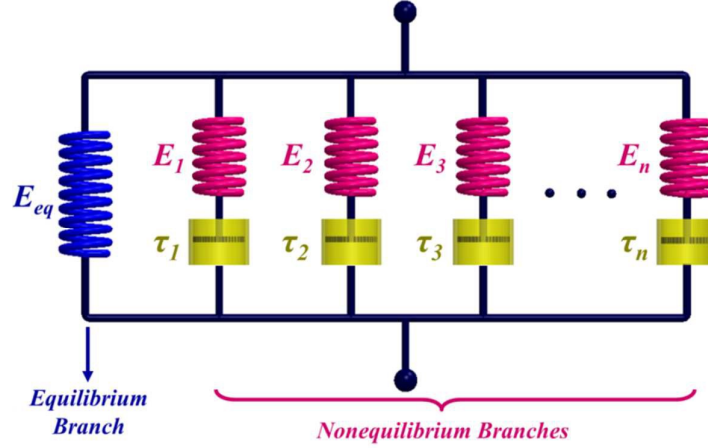
Figure 4. 1D rheological representation of the model

By applying the Boltzmann's superposition principle [40], the total stress $\sigma(t)$ of

the model is:

$$\sigma(t) = E_{eq}e_m(t) + \sum_{i=1}^{n} E_i e_i^e \tag{1a}$$

with

$$e_i^e = \int_0^t \frac{de_m(s)}{dt} \exp\left(-\int_s^t \frac{dt'}{\tau_i(T,t')}\right) ds, \tag{1b}$$

to describe the elastic strain evolution in each nonequilibrium branches. In Eq. 1a and

1b, $e_m(t)$ is the total strain. E_{eq} and E_i are the elastic modulus in the equilibrium

and nonequilibrium branches, respectively. $\tau_i(T)$ denotes the temperature dependent

relaxation time in the dashpots. The elastic energy stored in individual branches are

calculated as

$$U_i = \frac{1}{2}E_i\left(e_i^e\right)^2. \tag{1c}$$

Here, it is assumed that the time-temperature shift for each branch follows the

same rule. According to the well-established "thermorheological simplicity" principle [40] under a non-isothermal condition, the relaxation times (or viscosity) of each nonequilibrium branch vary as the temperature changes:

$$\tau_i = \alpha_T(T)\tau_i^0,\tag{2}$$

where $\alpha_T(T)$ is a time-temperature superposition (TTSP) shifting factor, and τ_i^0 is the reference relaxation time at the temperature when $\alpha_T(T) = 1$.

Following O'Connell and McKenna [41], the method for calculating the temperature influence on the viscoelastic behavior depends on whether the material temperature is above or below a shifting temperature T_s. For temperatures above and near T_s, the (Williams-Landel-Ferry) WLF equation is used to calculate $\alpha_T(T)$ [42]:

$$log\alpha_T(T) = -\frac{C_1(T - T_M)}{C_2 + (T - T_M)},\tag{3a}$$

where T_M is the WLF reference temperature, and C_1 and C_2 are material constants that depend on the choice of T_M. In comparison, for temperature below T_s, $\alpha_T(T)$ follows the Arrhenius-Type behavior [43]:

$$ln\alpha_T(T) = -\frac{AF_c}{k_b}\left(\frac{1}{T} - \frac{1}{T_g}\right),\tag{3b}$$

where A is a material constant, F_c is the configurational energy and k_b is Boltzmann's constant. The shifting temperature T_s is the crossing point of two curves representing Eqs. 3a and 3b on an $\alpha_T(T)$ vs T plot.

3.2 Model parameters identification

In our previous work [44], a detailed method was given to identify all the model parameters for applied epoxy SMP. Briefly, there are two groups of parameters in the

applied multi-branched model: the parameters in TTSP, and the elastic modulus and

relaxation time in each branch. The identification process of TTSP parameters is

described in the supplementary material (Section S1), where the DMA data and

temperature dependent stress relaxation (SR) data are used. The elastic modulus and

relaxation time in each branch are determined by fitting the DMA data as following.

By using nonlinear regression (NLREG) method [45, 46], the elastic modulus and

relation time in each branch is determined. For the 1D multi-branched linear model,

the temperature dependent storage modulus $E_s(T)$, loss modulus $E_l(T)$ and

$\tan \delta(T)$ are respectively expressed as:

$$E_s(T) = E_{eq} + \sum_{i=1}^{n} \frac{E_i w^2 \tau_i^2}{1 + w^2 \tau_i^2},\tag{4a}$$

$$E_l(T) = \sum_{i=1}^{n} \frac{E_i w \tau_i}{1 + w^2 \tau_i^2},\tag{4b}$$

$$\tan \delta(T) = \frac{E_l(T)}{E_s(T)},\tag{4c}$$

where w is the testing frequency. For the convenience of operation, we assume that

the relaxation times in the nonequilibrium branches increase in a tenfold sequential.

During the NLREG analysis, nonequilibrium branches are gradually added into the

model to improve the prediction, and the branch number is finally determined when

the NLREG estimations (shown as dash lines in Fig. 5) could capture the

experimental storage and tanδ curves within the entire testing temperature range

(25 °C-140 °C).

It should be noted that the model parameters are determined based on the results

from DMA tests with small strain amplitude (0.1%). Previous studies [47-51] showed

that the time scale of the polymer response also depends on the deformation, where the stress induced dilatation in polymer network will affect the mobility of molecular chains by changing the free volume. In the supplementary material (Section S2), the influence of deformation on shift factors is examined. It is seen that if the SMPs are deformed at temperatures greatly above T_g, the change of shift factors is minimal, which indicates that the free volume increment contributed from stress dilatation is small compared with that from thermal energy. In this paper, since both the cyclic tension and programming deformation of SMPs are performed at high temperatures, it is safe to assume that the relaxation times and thermodynamical behaviors of SMPs are not affected by the deformation.
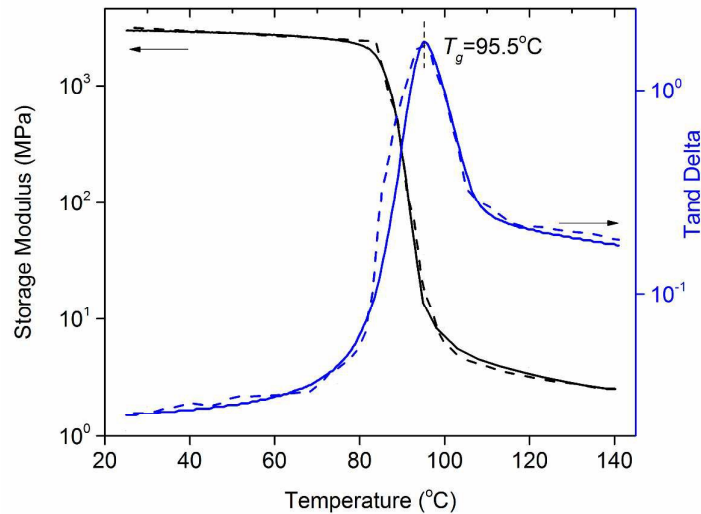
Figure 5. Comparisons between the storage modulus and tanδ curves. Solid lines denote experimental results and dash lines denote predictions.

By using the DMA data and temperature dependent SR data, all of the model parameters can be fully determined. The final set of parameters is listed in Table 1.

Table 1 Parameters of the applied constitutive model

Model Parameters	Parameter Value	Identification Method
Parameters in TTSP		

T_g (°C)	95					*Measured from DMA data*
T_M (°C)	85					*Measured from DMA data*
AF_c/k_b	-24500					*Fitted from SR data*
C_1	10.44					*Fitted from SR data*
C_2 (°C)	15.6					*Fitted from SR data*

Initial Moduli and Relaxation Times in Nonequilibrium Branches

$E^1 \sim E^{18}$ (MPa)	129.0	99.9	112.1	112.8	91.9	92.1	
	128.4	960.0	775.5	432.5	190.3	72.1	*Fitted from DMA data*
	5.6	2.7	0.9	0.5	0.4	1.5	
$\tau_0^1 \sim \tau_0^{18}$ (s)	1.0×10^{-7}	8.2×10^{-7}	5.8×10^{-6}	5.6×10^{-5}	3.4×10^{-4}	1.8×10^{-3}	
	1.5×10^{-2}	5.4×10^{-1}	1.0×10^{0}	8.4×10^{1}	5.9×10^{2}	3.7×10^{3}	*Fitted from DMA data*
	2×10^{4}	2×10^{5}	2×10^{6}	2×10^{7}	2×10^{8}	2×10^{9}	

Initial Modulus in Equilibrium Branch

E_{eq}	0.65					*Measured from DMA data*

4. Results and Discussions

4.1 Predictions on the cyclic stress-strain behaviors and shape memory behaviors

By using the multi-branched model and the pre-determined parameters in Table 1, the aforementioned cyclic tension and SM experiments were studied and the predicted results were compared with the experimental ones. In the following discussions, there is no further parameter adjustment or fitting process involved.

Fig. 6a shows the comparison of the stress-strain behavior from the results of the predictions and the tests. For the sake of clarity, we only plot the curves of the tension cycles 1, 2 and 10. It can be seen that the results predicted by the model are very close to the experimental results. The maximum stress before unloading and the residual

strain in each cycle are depicted in Fig. 6b. As predicted by the model, when the

number of cycle increases, the maximum tension stress in the sample becomes lower,

while the residual strain rises from 10% to 15.5%. However, both the maximum stress

and the residual strain will flatten out gradually as the number of cycle is increased to

a large value/magnitude.

(a)

(b)
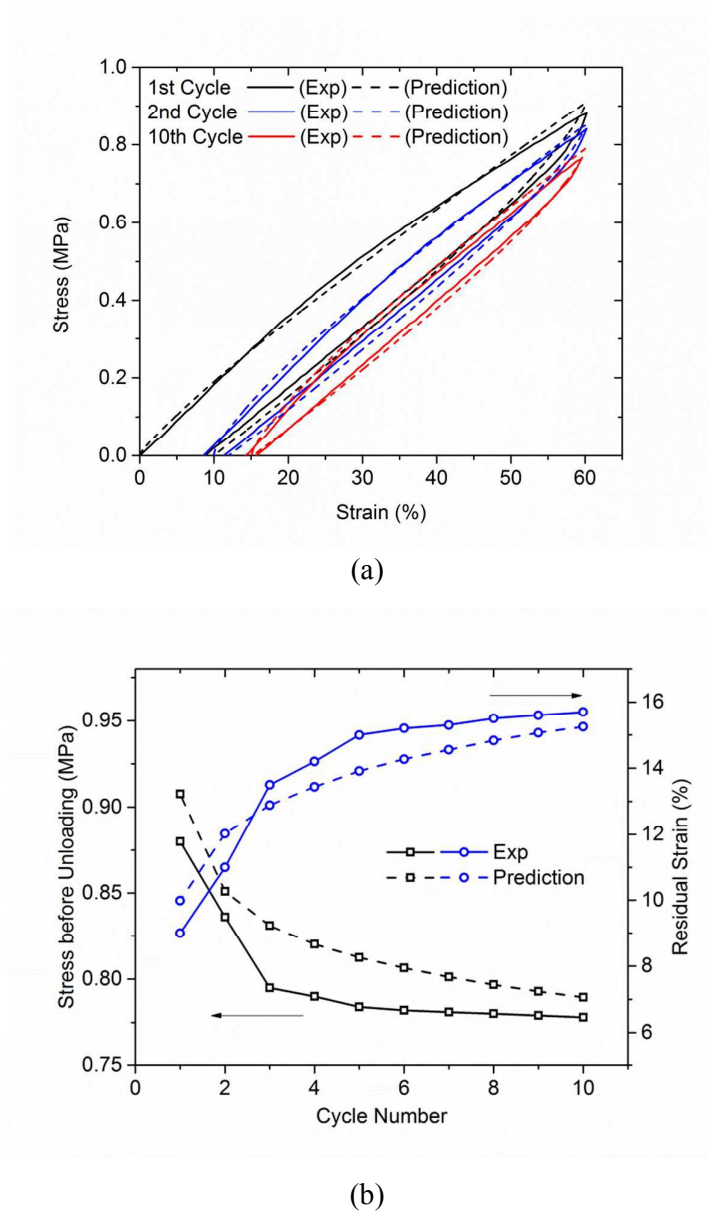
Figure 6. Comparison between experiments and model predictions for (a) the stress-strain curve (1st, 2nd and 10th cycles) at $120^{\circ}C$, and (b) the stress before unloading and residual strain as a function of cycle number.

The prediction results on the cyclic SM response are shown in Fig. 7a, which plots

the variations of the strains during the free recovery in cycles 1, 2, 6 and 10. It can be

seen that the predicted curves coincide with those of the experiment very well.

Furthermore, the shape fixity (R_f), average and total shape recovery ratio ($R_{r,ave}$ and

$R_{r,tot}$) are used as performance parameters for the fixing and recovery of the SMP.

They are defined as followings [40]

$$R_f = \frac{\varepsilon_u}{\varepsilon_p}, \tag{5a}$$

$$R_{r,ave} = \frac{\varepsilon_p - \varepsilon_f(N)}{\varepsilon_p - \varepsilon_f(N-1)}, \tag{5b}$$

$$R_{r,tot} = \frac{\varepsilon_p - \varepsilon_f(N)}{\varepsilon_p}, \tag{5c}$$

where ε_p is the prescribed axial strain, ε_u is the measured strain after unloading to zero

force before reheating the sample, and $\varepsilon_f(N)$ is the final axial strain at the end of cycle

N. It is noted that the total shape recovery ratio in Eq. 5c uses the original

pre-deformed configuration as the reference value, and therefore provides a measure

of the performance of the material in reference to its original state when cycled

multiple times, while the average recovery ratio in Eq. 5b describes the shape

recovery performance in the current SM cycle. These parameters determined from the

tests and predicted by the model in different cycles are plotted in Fig. 7b. It can be

seen that R_f almost remains constant (near 100%) and $R_{r,ave}$ increases slightly with the

number of cycles. The behavior of $R_{r,tot}$ is quite different; it decreases obviously as the

number of cycle increases.
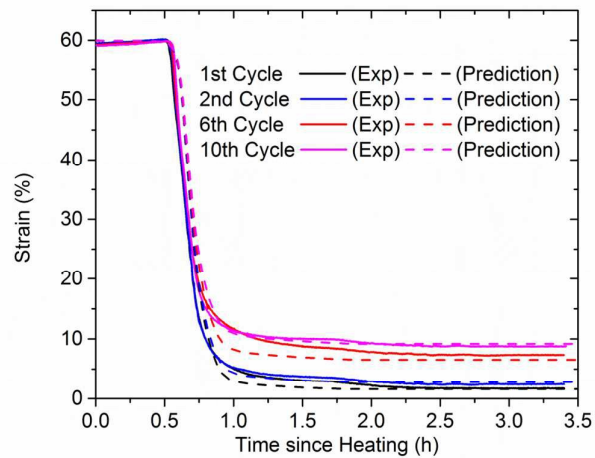
(a)
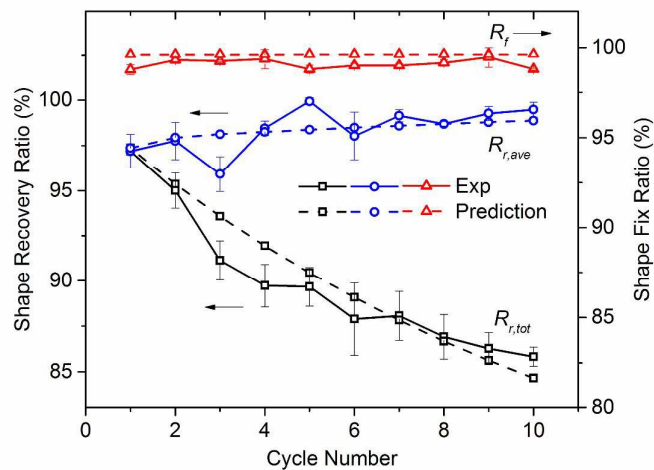
(b)

Figure 7. Comparisons between experiments and model predicrtions for the shape memory effects a) on the strain evolution during the recovery step (1st, 2nd, 6th and 10th cycles), b) on the shape fixity and recovery ratios as a function of cycle number.

4.2 Parametric Study on the cycling behaviors

The comparison between the experimental results and model prediction confirm that the observed deterioration in the cyclic thermomechanical and SM behaviors of SMPs are not caused by damage; it can be attributed to the viscoelastic nature of polymer studied in this work. Therefore, it is an interesting question that how can one

reduce or control the effect of this factor. In this section, the influences of different thermal-temporal conditions, such as loading rate, temperature and idle time between two cycles, on the cyclic behaviors of SMP are discussed by using the presented model for the Veriflex E epoxy SMP material.

The effect of loading rate is first examined on the cyclic tensile behavior of SMPs. The loading rate was changed as 0.2%/min, 2%/min, 20%/min and 200%/min, while the temperature during the tension was kept at 120°C. The idle time between two cycles is set to be zero, namely the stretching in each cycle is performed immediately when the unloading stress in the last cycle reduces to zero. The residual strain (Fig. 8a) and the peak stress (Fig. S2a) were predicted in each cycle with these loading rates. It is seen that the residual strain and the peak stress decrease significantly with the reduction of the loading rate. At a lower loading rate, the residual strain and the peak stress quickly reach a saturated level.

The effect of temperature was predicted during the cyclic tension. Fig. 8b and Fig. S2b show the residual strain and the peak stress versus the number of cycles when the temperature are set as 100°C, 110°C, 120°C and 130°C respectively and the loading rate remains 2%/min. It is seen that increasing the temperature plays the same role as decreasing loading rate. When the sample is stretched under a higher temperature, the decrease of the residual strain and the peak stress is significant, and these values saturate after the first few cycles.

These results indicate that to minimize the residual strain, it is beneficial to use a lower loading rate or a higher temperature. However, when such approaches are not

available options, such as in the medical or microelectromechanical applications where the loading rate and maximum temperatures might be restricted, one can choose to stabilize the material after unloading before proceeding to the next loading cycle. Within this idle time, the SMP is free standing at the loading temperature and will gradually recover the residual strain. Fig. 8c and Fig. 8d show the reduction of residual strain as a function of idle time. The idle temperature is the same as the corresponding loading temperatures (120 ^{o}C and 100 ^{o}C respectively). It is seen that at 120 ^{o}C, a 12s (0.2min) of idle time will reduce the residual strain by ~33% after 40 cycles (from 16.5% to 11%). If 30 min of idle time is given, the residual strain in the 40th loading cycle is reduced by 81.1% (from 16.5% to 3.1%). On the other hand, when the loading temperature is lower (100 ^{o}C in Fig. 8d), a longer idle time is required to reduce the same amount of residual strain due to the slower shape recovery.

(a) (b)

(c)   (d)
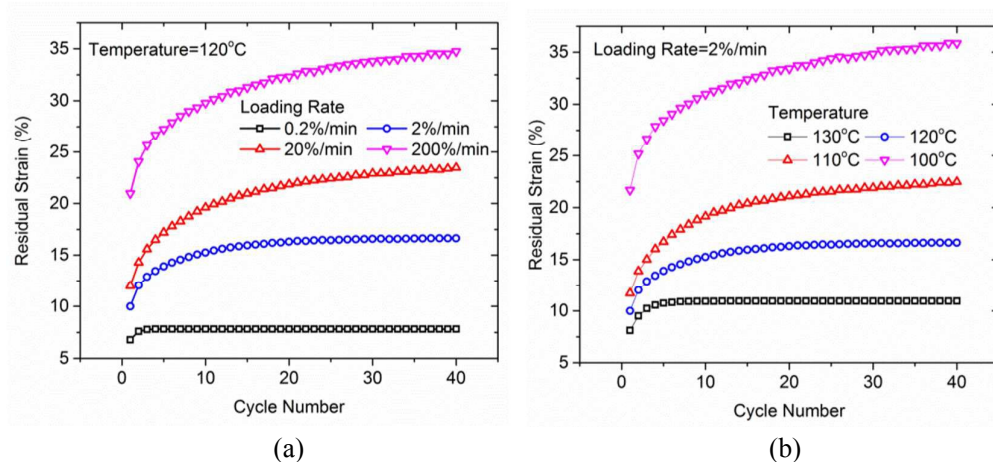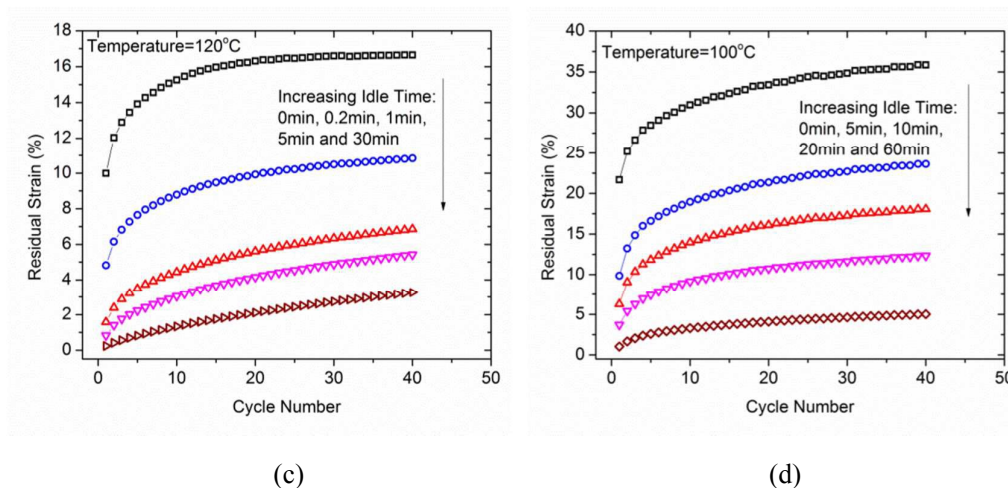
Figure 8. Model predictions to reveal the effects of (a) loading rates and (b) temperatures on the residual strain after unloading, and model predictions to reveal the effects of idle time on residual strain after unloading at (c) 120 °C and (d) 100 °C.

We then proceed to investigate the influence of thermal-temporal conditions on the cyclic SM behavior of SMPs. The simulation procedures are consistent with the experimental ones: In a typical SM cycle, the SMP was strained to 60% at the programming temperature (T_d) with a loading rate of 50 mm/min, and then held at T_d for a given time. Next, the sample was cooled to 25°C at a rate of 2.5°C/min while the strain was kept at 60%, after which the sample was held (at 25°C and 60% strain) for 60 min before unloading. The free recovery step consisted of heating the sample (again at 2.5°C/min) to the target recovery temperature (T_r) and idling at T_r for a given time. In this manner, the total recovery time of SMP equals the heating time plus the idle time at T_r. After that, the SMP was cooled back to 25°C (at 2.5°C/min), and finally stabilized at 25°C for 60 min.

We first examine the influence of holding time at T_d during the programming step. Both the programming temperature (T_d) and the recovery temperature (T_r) are set to be 130 °C, while the holding time after stretching is changed to 3s, 30s, 300s and

3000s, respectively. The idling time after the temperature reaching T_r is 60min (the same as that in experiments). Fig. 9a plots the total shape recovery ratio at the end of each SM cycle. It is seen that for each case of holding time, the recovery ratio first decreases and then tends to saturate at large cycling numbers.

In our previous work [37, 38], we demonstrated that the elastic strain energy in the multi-branched model is an appropriate parameter to examine the shape memory behavior. Since the viscoelastic properties of SMPs can be characterized by the energy storage and release, we further examine the strain energy distribution in the model to assist the study of cyclic behaviors. For the case of holding time being 3000s, we calculated the residual strain energy at the end of each SM cycle according to Eq. 1c. The top figure of Fig. 9b shows the residual strain energy at the end of 1st, 10th, 20th, 30th and 40th SM cycle (states ①-⑤ in Fig. 9a), where the strain energy in all non-equilibrium branches is added up. It is seen that due to incomplete shape recovery in each cycle, the residual strain gradually accumulates. Compared with the 1st SM cycle, the residual strain energy in the equilibrium branch after the 40th cycle is increased by 15.7 times (from $\sim 2.3 \times 10^3$ J/m^3 to 3.6×10^4 J/m^3). The residual strain energy after each SM cycle is proportional to the residual strain.

Fig. 9a also shows that reducing the holding time will increase the total shape recovery ratio. The bottom figure of Fig. 9b plots the residual strain energy after the 40th cycle with different holding time, which is corresponding to the states ⑤-⑧ in Fig. 9a. When the holding time after the programming deformation is reduced from 3000s to 3s, $R_{r,tot}$ in the 40th cycle is improved from $\sim 44\%$ to $\sim 90\%$, and the residual

strain energy in the equilibrium branch is reduced from 3.6×10^4 J/m^3 to 2.1×10^3 J/m^3,

which indicates a slower accumulation of residual strain energy. This observation can

be explained by our previous study on the polymer temperature memory effect [37]:

when a small holding time is given, the polymer chains do not have enough

stabilization time to adjust their conformation in compliance with the programming

deformation. In this manner, significant elastic strain energy will be stored within the

network, which provides additional driving force for the free recovery, and hence the

recovery ratio is increased at a given recovery temperature. The analysis on the effect

of decreasing holding time can be extended to the influence of other thermo-temporal

programming conditions, such as increasing loading rate, cooling rates, or decreasing

the programming temperature etc.
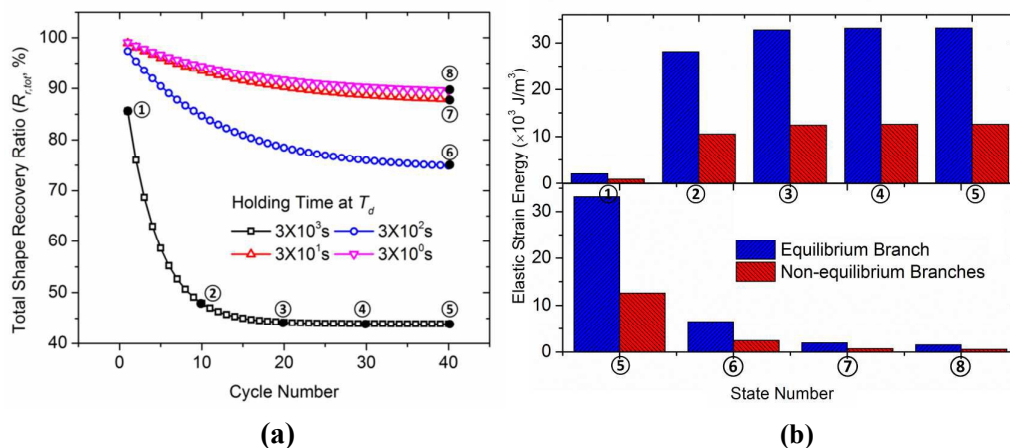
Figure 9. (a) The predicted total shape recovery ratio as a function of holding time and cycle number. Programming temperature and recovery temperature are both 130°C. **(b)** The predicted residual elastic strain energy distribution at the ends of different cycles for holding time is 3000s. **(c)** The predicted residual elastic strain energy distribution at the end of 40th cycle for different holding time.

Next, the influence of the recovery temperature (T_r) on the cyclic SM behavior is

investigated. The total shape recovery ratios with different T_r (100°C, 110°C, 120°C,

130°C and 140°C) are predicted and plotted versus cycle time in Fig. 10a, where the programming conditions are set to be uniform in each case (programming temperature=130°C, holding time=300s and idle time at T_r=60min). For the case of T_r =100°C, The top figure of Fig. 10b shows the residual strain energy in the multi-branched model at the end of 1st, 10th, 20th, 30th and 40th SM cycle, which is corresponding to the states ①-⑤ in Fig. 10a. The strain energy distribution at the end of the 40th SM cycle for each case of recovery temperature is plotted in the bottom figure of Fig. 10b, which is corresponding to the states ⑤ -⑨ in Fig. 10a.

It is seen that the residual strain energy increases quickly as the SM cycle proceeds. Compared with the 1st SM cycle, the strain energy in the equilibrium branch is increased from ~1.5×10⁴ J/m³ to ~ 5.6×10⁴ J/m³ at the end of the 40th SM cycle. This accumulated strain energy within the polymer network leads to the gradually reduced total recovery ratio at a given recovery temperature. On the other hand, Fig. 10a also reveals that the higher the recovery temperature, the larger the total shape recovery ratio, and earlier to reach the saturated level. For example, when the recovery temperature is increased from 100 °C to 140 °C, the total recovery ratio in the 40th SM cycle is increased from ~30% to ~ 91% and the residual strain energy in the equilibrium branch is reduced from 5.6×10⁴ J/m³ to 8.1×10² J/m³. The results in Fig. 10 indicate a higher recovery temperature will help to suppress the accumulation of residual energy in the polymer network and improve the cyclic SM behavior of SMPs.

(a) **(b)**
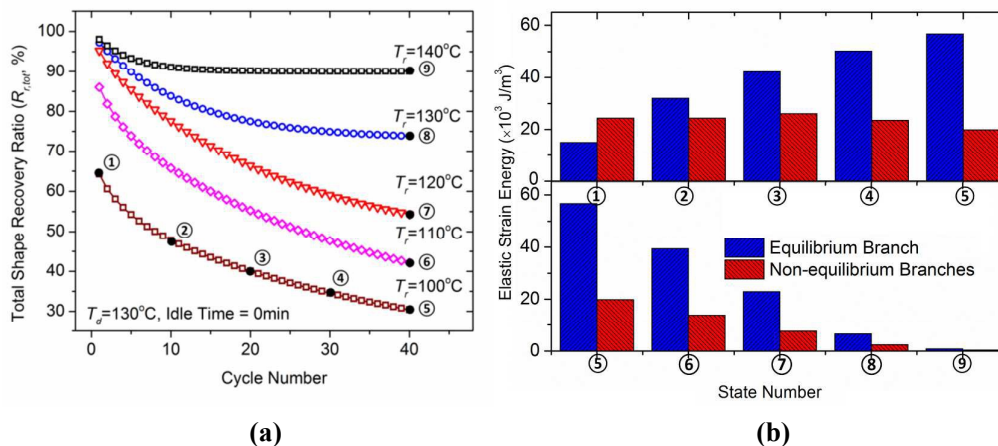
Figure 10. (a) The predicted total shape recovery ratio plot as a function of recovery temperature and cycle time. Hold time is 300s, T_d =130°C and Idle time between two SM cycle is zero. **(b)** The predicted residual elastic strain energy distribution at the ends of different cycles for shape recovery temperature is 100°C. **(c)** The predicted residual elastic strain energy distribution at the end of 40th cycle for different shape recovery temperature.

In the above discussion, the idle time at T_r is set to be 60min in each case. In the following, we further examine its influence on the cycle SM behaviors. Fig. 11a shows the total shape recovery ratio plot as a function of idle time and cycle number, where programming temperature T_d=130°C, the hold time at T_d is 300s, and the recovery temperature T_r=100°C, while the idle time at T_r is changed as 1min, 10min, 60min, 600min, 6000min and 21201min. It is seen that increasing the idle time is equivalent to increasing the recovery temperature in reducing the decay of recovery ratio and improving the cyclic SM behavior. When the idle time is only 1min, the total recovery ratio is below 10% within the 40 SM cycles. After increasing the idle time to 21201min (~14.7 days), the total shape recovery ratio at the end of 40th SM cycle is increased to 72%, which is equivalent to that in Fig. 10a with idle time=60min and T_r=130°C. Such an equivalency is a reflection of the classic time-temperature superposition principle, and can be characterized by using our previous study on

25

reduced time [36], namely if the SMPs are programmed at the same thermal-temporal

condition, the recovery ratio can be uniquely determined by the reduced recovery time

t_r:

$$t_r = \int_0^t \frac{ds}{\alpha(T)}, \qquad (6)$$

where t is the physical recovery time (the heating time plus idling time) and T is the

temperature evolution during the free recovery step, and $\alpha(T)$ is the shift factors

defined in Eq. 3. Based on Eq. 6, we are able to calculated an equivalent idle time at

different recovery temperatures where the SMP has the same reduced recovery time t_r

and total recovery ratio. Fig. 11b shows the equivalent idle time at T_r=130°C as a

function of idle time at T_r=100°C. It is seen that these two idle times exhibit an almost

linear relation, and the required idle time at T_r=130°C is only 375 times smaller than

that at T_r=100°C in order to achieve the same level of total shape recovery ratio.

(a)   (b)
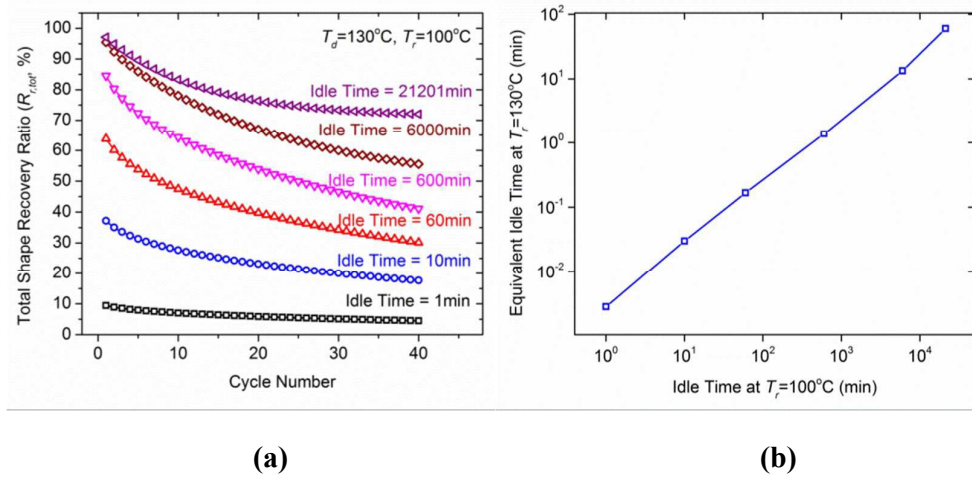
Figure 11. (a) The predicted total shape recovery ratio as a function of idle time and cycle time. Hold time is 300s, T_d=130°C and T_r=100°C. **(b)** The equivalent idle time at T_r=130°C as a function of idle time at T_r=100°C.

As seen in Fig. 1, the glass transition of epoxy SMP spans from ~70°C to ~140 °C ,

and the material remains significantly viscous at higher temperature, which is the

main reason for the demonstrated deterioration in cyclic SM behaviors. Here, we investigate how the thermomechanical behaviors, particularly the width of glass transition, can affect the cyclic SM behaviors of SMP. To demonstrate this, parametric studies are conducted on the TTSP parameters, such as C_1, C_2, AF_c/k_b, while the programming and recovery conditions are set to be identical in each case (T_d=130°C, the hold time at T_d=300s, T_r=100°C and idle time at T_r=60min). The goal of parameter adjustment is to tune the glass transition range, while fixing the T_g always at 95 °C. As shown in Fig. 12a, when C_1, C_2, AF_c/k_b are set to be 11.24, 0.2 °C and -24500 respectively, the transition region is narrowed down to ~80°C to ~110°C. The corresponding total shape recovery ratio at T_r=100°C is almost 100% for each SM cycle (see Fig. 12b), which indicates a significant improvement in the cyclic SM performance. On the other hand, when C_1, C_2, AF_c/k_b are set to be 11.24, 80.6 °C and -2450 respectively, the tan δ remains high within the entire temperature range, and the corresponding total shape recovery ratio is stabilized at ~30% during the 40 SM cycles.

(a)   (b)
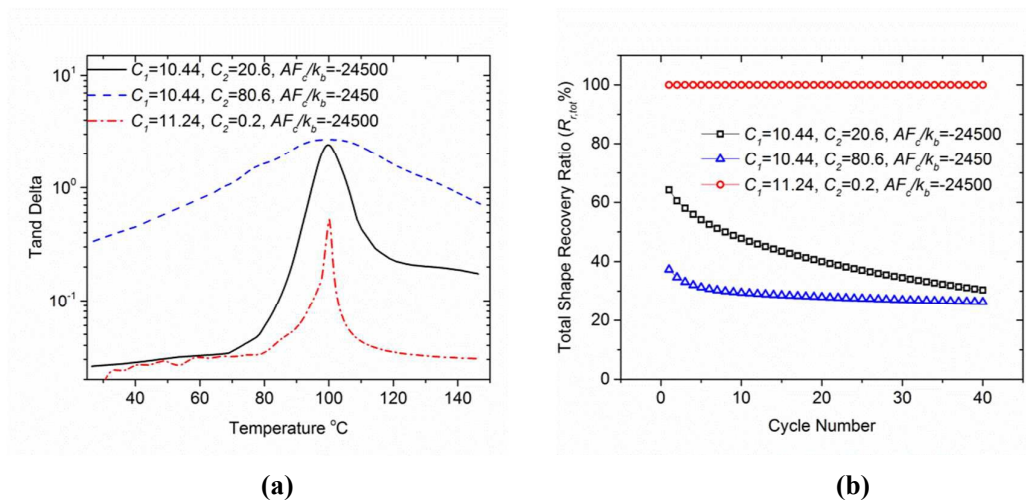
Figure 12 (a). Predicted tanδ curves with different C_1, C_2, AF_c/k_b being applied. Other model

parameters are the same as listed in Table 1 **(b)**. The predicted total shape recovery ratio as a function of cycle number. The recovery temperautre is 100°C for each case.

It is also possible to improve the cyclic SM behavior by just increasing E_{eq}. Fig. 13a shows the predicted tanδ curves with different equilibrium moduli (E_{eq} =0.65MPa, 2MPa, 5MPa and 10MPa respectively) being applied in the multi-branched model. It is seen that the high-temperature viscous nature of the epoxy SMP is minimized, and the tanδ is reduced from ~0.13 to ~0.01 when E_{eq} is increased to 10 MPa. Consequently, the total shape recovery ratio at T_r=100°C is increased from ~30% to ~80% after the 40th SM cycle (see Fig. 13b). The demonstrated methods (narrowing the glass transition range or increasing E_{eq}) in improving the cyclic SM behaviors can be realized by tuning material properties. For example, the glass transition range can be synthetically controlled and is related to the heterogeneity (both structurally and dynamically) of the polymer, and a higher E_{eq} can be realized by increasing the crosslink density of the epoxy[52].

(a)   (b)
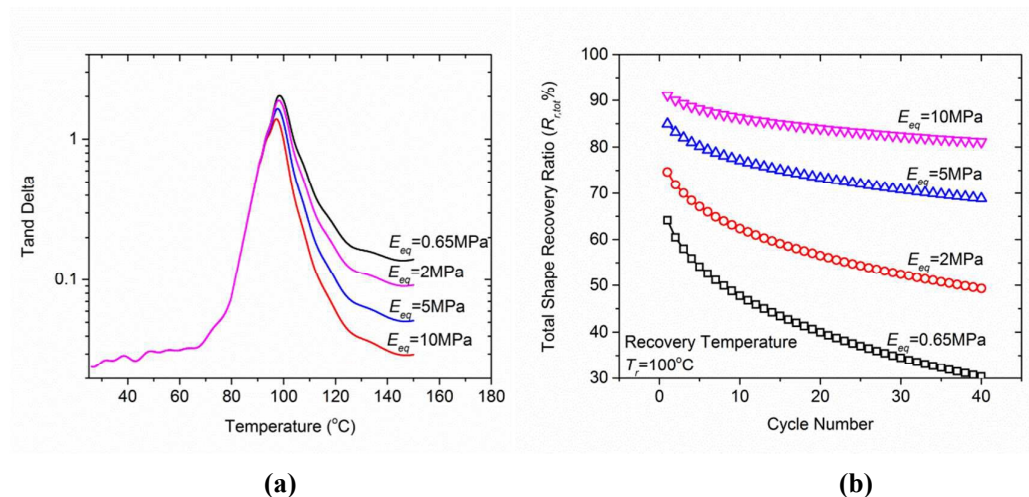
Figure 13. (a). Predicted tanδ curves with different E_{eq} being applied. Other model parameters are the same as listed in Table 1 **(b)**. The predicted total shape recovery ratio as a function of E_{eq} and cycle number. The recovery temperautre is 100°C for each case.

5. Conclusion

In this paper, we explored the influence of viscoelastic properties on the cyclic thermomechanical and shape memory (SM) behaviors of amorphous shape memory polymers (SMPs). The investigated epoxy thermosetting polymer, with no visible damage or irreversible softening effect during the deformation, still exhibits obvious degradation in the cyclic tension and SM behaviors, which is attributed to its viscoelastic nature even at temperatures greatly above its transition temperature (T_g). A multi-branched model is utilized to assist the understanding of the mechanical responses of amorphous SMPs. The model is validated by the comparisons between the model predictions and the results of the cyclic tension and SM tests. Parametric studies are carried out to quantitatively investigate the influence of viscoelastic behaviors of SMPs on their cyclic thermomechanical behaviors. The results suggest that the cyclic shape memory and recovery performance can be improved by adjusting programming and recovery conditions, such as lowering the loading rate, raising the programming temperature, reducing the holding time and increasing the idle time at high temperature. In particular, stabilizing the SMP at a high temperature between two SM cycles, which gives the material enough time to recover, can significantly reduce the decay in recovery ratio. Our parametric studies also show that narrowing the temperature range of glass transition and increasing the equilibrium modulus of the SMPs can reduce the performance decay under cyclic SM conditions.

Acknowledgement

References

1.   Behl, M., et al., *One-Step Process for Creating Triple-Shape Capability of AB Polymer Networks.* Advanced Functional Materials, 2009. **19**(1): p. 102-108.

2.   Luo, X.F. and P.T. Mather, *Triple-Shape Polymeric Composites (TSPCs).* Advanced Functional Materials, 2010. **20**(16): p. 2649-2656.

3.   Xie, T., *Tunable polymer multi-shape memory effect.* Nature, 2010. **464**(7286): p. 267-270.

4.   Liu, C., H. Qin, and P.T. Mather, *Review of progress in shape-memory polymers.* Journal of Materials Chemistry, 2007. **17**(16): p. 1543-1558.

5.   Gall, K., et al., *Thermomechanics of the shape memory effect in polymers for biomedical applications.* Journal of Biomedical Materials Research Part A, 2005. **73A**(3): p. 339-348.

6.   Mohr, R., et al., *Initiation of shape-memory effect by inductive heating of magnetic nanoparticles in thermoplastic polymers.* Proceedings of the National Academy of Sciences of the United States of America, 2006. **103**(10): p. 3540-3545.

7.   Schmidt, A.M., *Electromagnetic activation of shape memory polymer networks containing magnetic nanoparticles.* Macromolecular Rapid Communications, 2006. **27**(14): p. 1168-1172.

8.   Lendlein, A., et al., *Light-induced shape-memory polymers.* Nature, 2005. **434**(7035): p. 879-882.

9.   Scott, T.F., et al., *Photoinduced plasticity in cross-linked polymers.* Science, 2005. **308**(5728): p. 1615-1617.

10.   Huang, W.M., et al., *Water-driven programmable polyurethane shape memory polymer: Demonstration and mechanism.* Applied Physics Letters, 2005. **86**(11): p. -.

11.   Yakacki, C.M., et al., *Unconstrained recovery characterization of shape-memory polymer networks for cardiovascular applications.* Biomaterials, 2007. **28**(14): p. 2255-2263.

12.   Lendlein, A. and S. Kelch, *Shape-memory polymers as stimuli-sensitive implant materials.* Clinical Hemorheology and Microcirculation, 2005. **32**(2): p. 105-116.

13.   Francis, W.H., et al. *Elastic Memory Composite Microbuckling Mechanics: Closed-Form Model with Empirical Correlation.* in *48th AIAA/ASME/ASCE/AHS/ASC Structures, Structural Dynamics, and Materials Conference.* 2007. Honolulu, Hawaii.

14.   Gall, K., et al., *Shape-memory polymers for microelectromechanical systems.* Journal of Microelectromechanical Systems, 2004. **13**(3): p. 472-483.

15.   Ohki, T., et al., *Mechanical and shape memory behavior of composites with shape memory polymer.* Composites Part a-Applied Science and Manufacturing, 2004. **35**(9): p. 1065-1073.

16.   Shojaei, A., G.Q. Li, and G.Z. Voyiadjis, *Cyclic Viscoplastic-Viscodamage Analysis of Shape Memory Polymers Fibers With Application to Self-Healing Smart Materials.* Journal of Applied Mechanics-Transactions of the Asme, 2013. **80**(1).

17.   Shojaei, A., G.Z. Voyiadjis, and P.J. Tan, *Viscoplastic constitutive theory for brittle to ductile damage in polycrystalline materials under dynamic loading.* International Journal of Plasticity, 2013. **48**: p. 125-151.

18.   Di Prima, M.A., et al., *Cyclic compression behavior of epoxy shape memory polymer foam.* Mechanics of Materials, 2010. **42**(4): p. 405-416.

19.   John, M. and G.Q. Li, *Self-healing of sandwich structures with a grid stiffened shape memory polymer syntactic foam core.* Smart Materials & Structures, 2010. **19**(7).

20.   Li, G.Q. and A. Shojaei, *A viscoplastic theory of shape memory polymer fibres with application to self-healing materials.* Proceedings of the Royal Society a-Mathematical Physical and Engineering Sciences, 2012. **468**(2144): p. 2319-2346.

21.   Li, G.G. and N. Uppu, *Shape memory polymer based self-healing syntactic foam: 3-D confined thermomechanical characterization.* Composites Science and Technology, 2010. **70**(9): p. 1419-1427.

22.   Shojaei, A., G. Li, and G.Z. Voyiadjis, *Cyclic Viscoplastic-Viscodamage Analysis of Shape Memory Polymers Fibers With Application to Self-Healing Smart Materials.* Journal of Applied Mechanics, 2013. **80**: p. 01101401-01101415.

23.   Shojaei, A. and G.Q. Li, *Thermomechanical constitutive modelling of shape memory polymer including continuum functional and mechanical damage effects.* Proceedings of the Royal Society a-Mathematical Physical and Engineering Sciences, 2014. **470**(2170).

24.   Nji, J. and G.Q. Li, *A self-healing 3D woven fabric reinforced shape memory polymer composite for impact mitigation.* Smart Materials & Structures, 2010. **19**(3).

25.   Bianchi, O., et al., *Assessment of Avrami, Ozawa and Avrami–Ozawa equations for determination of EVA crosslinking kinetics from DSC measurements.* Polymer Testing, 2008. **27**(6): p. 722-729.

26.   Qi, H.J., et al., *Finite deformation thermo-mechanical behavior of thermally induced shape memory polymers.* Journal of the Mechanics and Physics of Solids, 2008. **56**(5): p. 1730-1751.

27.   Li, G.Q. and W. Xu, *Thermomechanical behavior of thermoset shape memory polymer programmed by cold-compression: Testing and constitutive modeling.* Journal of the Mechanics and Physics of Solids, 2011. **59**(6): p. 1231-1250.

28.   Nguyen, T.D., et al., *A thermoviscoelastic model for amorphous shape memory polymers: Incorporating structural and stress relaxation.* Journal of the Mechanics and Physics of Solids, 2008. **56**(9): p. 2792-2814.

29.   Xu, W. and G.Q. Li, *Thermoviscoplastic Modeling and Testing of Shape Memory Polymer Based Self-Healing Syntactic Foam Programmed at Glassy Temperature.* Journal of Applied Mechanics-Transactions of the Asme, 2011. **78**(6).

30.   Yu, K., Q. Ge, and H.J. Qi, *Effects of stretch induced softening to the free recovery behavior of shape memory polymer composites.* Polymer, 2014. **55**(23): p. 5938-5947.

31.   Tobushi, H., S. Hayashi, and S. Kojima, *Mechanical-Properties of Shape-Memory Polymer of Polyurethane Series.* Proceedings of the 1993 Sem 50th Anniversary Spring Conference on Experimental Mechanics, 1993: p. 520-527.

32.   Poilane, C., et al., *Analysis of the mechanical behavior of shape memory polymer membranes by nanoindentation, bulging and point membrane deflection tests.* Thin Solid Films, 2000. **379**(1-2): p. 156-165.

33.   McClung, A.J.W., G.P. Tandon, and J.W. Baur, *Strain rate- and temperature-dependent tensile properties of an epoxy-based, thermosetting, shape memory polymer (Veriflex-E).* Mechanics of Time-Dependent Materials, 2012. **16**(2): p. 205-221.

34.   McClung, A.J.W., G.P. Tandon, and J.W. Baur, *Deformation rate-, hold time-, and cycle-dependent shape-memory performance of Veriflex-E resin.* Mechanics of Time-Dependent Materials, 2013. **17**(1): p. 39-52.

35.   Qi, H. and M. Boyce, *Stress-strain behavior of thermoplastic polyurethanes.* Mechanics of Materials, 2005. **37**(8): p. 817-839.

36.   Yu, K., G. Qi, and H.J. Qi, *Reduced time as a unified parameter determining fixity and free recovery of shape memory polymers.* Nature communications, 2014. **5**: p. 3066.

37.   Yu, K. and H.J. Qi, *Temperature Memory Effect in Amorphous Shape Memory Polymers.* Soft Matter, 2014.

38.   Yu, K., et al., *Mechanisms of multi-shape memory effects and associated energy release in shape memory polymers.* Soft Matter, 2012. **8**(20): p. 5687-5695.

39.   Westbrook, K.K., et al., *A 3D Finite Deformation Constitutive Model for Amorphous Shape Memory Polymers: A Multi-Branch Modeling Approach for Nonequilibrium Relaxation Processes,.* 2010: p. Submitted.

40.   Rubinstein, M. and R.H. Colby, *Polymer physics.* 2003, New York: Oxford University Press, Oxford.

41.   O'Connell, P.A. and G.B. McKenna, *Arrhenius-type temperature dependence of the segmental relaxation below T-g.* Journal of Chemical Physics, 1999. **110**(22): p. 11054-11060.

42.   Williams, M.L., R.F. Landel, and J.D. Ferry, *Temperature Dependence of Relaxation Mechanisms in Amorphous Polymers and Other Glass-Forming Liquids.* Physical Review, 1955. **98**(5): p. 1549-1549.

43.   Di Marzio, E.A. and A.J.M. Yang, *Configurational entropy approach to the kinetics of glasses.* Journal of Research of the National Institute of Standards and Technology, 1997. **102**(2): p. 135-157.

44.   Zalar, P., et al., *Increased Mobility Induced by Addition of a Lewis Acid to a Lewis Basic Conjugated Polymer.* Advanced Materials, 2014. **26**(5): p. 724-727.

45.   Diani, J., et al., *Predicting thermal shape memory of crosslinked polymer networks from linear viscoelasticity* International Journal of Solids and Structure, 2012. **49**(5): p. 793-799.

46.   Sherrod, P.H. *Nonlinear Regression Analysis Program, NLREG Version 5.0.* 2000; Available from: http://www.nlreg.com/.

47.   Knauss, W.G. and I.J. Emri, *Non-Linear Viscoelasticity Based on Free-Volume Consideration.* Computers & Structures, 1981. **13**(1-3): p. 123-128.

48.   Ferry, J.D. and R.A. Straton, *The free volume interpretation of the dependence of viscosities and visco-elastic relaxation times on concentration, pressure and tensile strain.* Kolloid-Z, 1960. **171**(2): p. 107–111.

49.   Turnbull, D. and M.H. Cohen, *Free-volume model of the amorphous phase-glass transition.* J. Chem. Phys., 1961. **34**(1): p. 120.

50.   Quach, A. and R. Simha, *Pressure-volume-temperature properties and transitions of amorphous polymers; polystyrene and poly (orthomethylstyrene).* J. Appl. Phys., 1971. **82**(12): p. 4592–4606.

51.   Fillers, R.W. and N.W. Tschoegl, *The effect of pressure on the mechanical properties of polymers.* Trans. Soc. Rheology,, 1977. **21**(1): p. 51-100.

52.   Ge, Q., et al., *Prediction of temperature-dependent free recovery behaviors of amorphous shape memory polymers.* Soft Matter, 2012. **8**(43): p. 11098-11105.